A Comparative Analytical Study for the Different Water Pools Present in Alginate Hydrogels: Qualitative vs. Quantitative Approaches

Mustapha El Hariri El Nokab [a]*, Julien Es Sayed [b], Fien De Witte [c], Koen Dewettinck [c], Ahmed Elshewy [d, e], Zhenlei Zhang [f], Paul H. M. Van Steenberge [g], Tuo Wang [a], Khaled O. Sebakhy [g]*

[a] Department of Chemistry, Michigan State University, East Lansing, MI 48824, USA.

[b] Zernike Institute for Advanced Materials (ZIAM), University of Groningen, Nijenborgh 4, 9747 AG, the Netherlands.

[c] Food Structure & Function Research Group, Ghent University, Coupure Links 653, 9000 Ghent, Belgium.

[d] Department of Pharmaceutical Organic Chemistry, Faculty of Pharmacy, Cairo University, 11562 Cairo, Egypt.

[e] Department of Medicinal Chemistry, Faculty of Pharmacy, Galala University, New Galala 43713, Egypt.

[f] College of Chemical Engineering and Environment, China University of Petroleum, Beijing 102249, P. R. China.

[g] Laboratory for Chemical Technology (LCT), Department of Materials, Textiles and Chemical Engineering, Ghent University, Technologiepark 125, 9052 Ghent, Belgium.

* Correspondence: elhariri@msu.edu; khaled.sebakhy@ugent.be

Abstract

Alginate hydrogels have garnered significant attention due to their promising applications in the food, biomedical, and pharmaceutical industries. The detection and quantification of distinct water phases within these hydrogels offer valuable insights into their dynamic, absorptive, and mechanical properties. Despite being comprised solely of 2 wt. % polymeric materials, the alginate hydrogels exhibit a highly porous morphology, characterized by distinct water pools exhibiting varying mobility and dynamic behaviors. These phases can be delineated as largely free water phase with high mobility, which occupies the macropores, and bound water with restricted mobility, which interacts with the fibrous polymeric structure. Water pools interacting with their surrounding environments possess variable crystal structures on variable freezing points, this could be easily detected using X-ray scattering techniques. A comparative study was conducted based on the information derived from each technique, with differential scanning calorimetry (DSC) yielding quantitative information for the water phases in alginate hydrogels (i.e., 58 % free and 42 % bound water in 0.75 wt. % - 6 h aging sample), whereas cryogenic scanning electron microscopy (Cryo-SEM), wide and small-angle X-ray scattering (WAXS and SAXS), Fourier Transform Infrared (FT-IR), and rheology provided valuable qualitative insights. In this study, deep insights into the molecular structure of alginates were obtained including the alteration in morphology and macropore

distribution, increase in the wall thickness, density, and mechanical properties upon increasing the Ca^{2+} concentration and aging period.

Keywords: Alginate, hydrogels, water phases, macropores, interconnected fibrous structure, quantitative analysis, qualitative analysis, drug delivery applications

1. Introduction

Alginates are natural polysaccharides obtained from brown seaweed (Abka-khajouei et al., 2022). Naturally extracted alginate consist of linear polyanionic polysaccharide chains connected through a 1-4 glycosidic linkage between α-guluronic acid (G) and β-mannuronic acid (M) (Saji et al., 2022). These chains consist of homopolymeric blocks of either G or M (poly-MM or poly-GG), as well as heteropolymeric blocks formed by alternating M and G residues (poly-MG) (Sharma et al., 2023). Alginates have the capacity to create hydrogels with a substantial water content when combined with divalent cations, such as Ca^{2+}, which facilitates the crosslinking of alginate polymeric chains, to form three-dimensional hydrophilic gel matrices (Daemi and Barikani, 2012; Nagaraja et al., 2021). Alginate hydrogels are well known in the food (Gheorghita Puscaselu et al., 2020) and biomedical industry (Hoffman, 2012) including drug delivery (Tønnesen and Karlsen, 2002), tissue engineering (Sharma et al., 2023), regeneration of cartilages (Neves et al., 2020), 3D bioprinting and wound healing due to their high-water content, biocompatibility, biodegradability, and cell encapsulation (Andersen et al., 2015; Tønnesen and Karlsen, 2002).

The ultimate properties of alginate materials are regulated by a variety of factors such as the chemical structure of carbohydrate constituents, the molecular weight of polymeric chain, the concentration of ions for crosslinking, the extent of hydration and the mobility of the matrix (Urbanova et al., 2019). Hence, in the design of a drug delivery system employing alginate for encapsulating membranes, nanoparticles, beads, thin films or scaffolds (Tønnesen and Karlsen, 2002), the controlled degree of hydration (Forgács et al., 2021), and the various water phases present, along with the exchange processes between these water phases and their surroundings, significantly influence the self-assembly and hydrocolloidal organization of alginate molecules and subsequently impact their viscosity (Akamatsu et al., 2011).

The content, distribution and dynamics of water molecules play a crucial role in regulating the overall chemical and physical properties of the resulting hydrogel (Ostrowska-Czubenko and Gierszewska-Drużyńska, 2009). The significance of the water composition within the hydrogel becomes evident through the valuable insights it offers into phenomena such as

swelling behavior, transport of nutrients and drugs, mobility, dynamic equilibrium, exchange processes within various water phases in the hydrogels, their interactions with the external environment, and numerous diffusive properties (Gun'ko et al., 2017; Hoffman, 2012; Rossi et al., 2015). To date, insufficient research has been conducted, and limited focus has been given to this subject, even though water may constitute as much as 99.9 wt. % of the hydrogel. Recently, two distinct water phases within alginate hydrogels have been identified using solid-state nuclear magnetic resonance (ssNMR) spectroscopy (El Hariri El Nokab, 2023; El Hariri El Nokab et al., 2022). These phases exhibit divergent chemical shifts, NMR relaxational behaviors, and line broadening characteristics. The aging period has shown significant effect on the molecular structure of the alginate hydrogel, where upon aging the pore formation and distribution increases thus resulting in the alteration and increase in free water ratio, of the water phase ratios.

Many analytical techniques have been established for investigating water characteristics in polymeric biomaterials, including polysaccharide hydrogels (Cavalieri et al., 2006; Gun'ko et al., 2017). The most reliable approach involves the combined use of multiple qualitative and quantitative techniques to assess water content and environments. These techniques encompass spectroscopic methods, such as ssNMR for studying water phases in neurodegenerative diseases, poly-peptides and chitosan films (Böckmann et al., 2009; Capitani et al., 2001; El Hariri El Nokab and van der Wel, 2020; Wang et al., 2017), pulsed field gradient diffusion NMR for studying water and ion diffusion into interpenetrating polymeric networks (Meo et al., 2021), FT-IR for investigating the structural changes occurring during hydrogel formation (Garcia et al., 2008; Pasqui et al., 2012; Roget et al., 2021) and Raman spectroscopy for studying the hydrophilic/hydrophobic interaction and degree of entanglement for gel formation (Rossi et al., 2015). Additionally, diffraction and X-ray scattering techniques provide information on the hydrogen bonding arrangements and their heat conduction in hydrogels through dynamical inter-molecular interactions (Naohara et al., 2017; Zhou et al., 2020) are employed, as well as other methods, including differential scanning calorimetry for quantifying the different water phases and their freezing behaviors (DSC) (Buchtová et al., 2018; Miyazaki et al., 2002; Panagopoulou et al., 2013), Quasi-elastic neutron scattering (Noferini et al., 2019), Cryo-electron tomography shows the crystalline liquid phases (Demurtas et al., 2015), Cryo-SEM provides information on the morphological and pores structures available (Aston et al., 2016; Buchtová et al., 2018). Small molecular probes investigate the flowability and diffusability of small nanoparticles in the

interconnected fibers and biofilms structures (Amsden, 1998; Rodríguez-Suárez et al., 2020), thermogravimatric analysis examines the thermal degradation and water dehydration of polymeric materials (Ostrowska-Czubenko and Gierszewska-Drużyńska, 2009) and rheology assesses the mechanical properties and density (Liparoti et al., 2021).

The formation of alginate hydrogels, as depicted in **Scheme 1**, and its physical and chemical properties are affected by several conditions including, but not limited to, the crosslinking ion concentration, pH, temperature, and aging period (Agulhon et al., 2012; Bhujbal et al., 2014; Brus et al., 2017; Forgács et al., 2021; Urbanova et al., 2019). The tuning of these variables affects the ratios of water phase inside the alginate hydrogel.

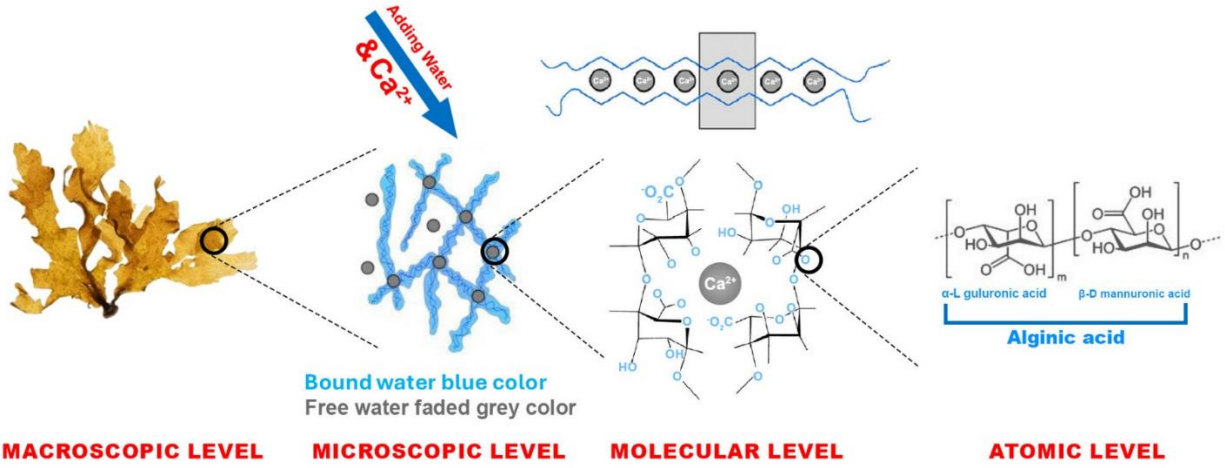

Scheme 1. Schematic representation of the formation of alginate hydrogels via calcium ions crosslinking extracted from brown seaweed.

2. Experimental Section

2.1. Alginate hydrogel sample preparation

Twelve alginate samples were prepared according to the procedure reported in our previous work (El Hariri El Nokab et al., 2022). Briefly, Alginate gels were prepared by dissolving alginic acid sodium salt (Sigma Aldrich, CAS: 9005-38-3) in D_2O-based NaOH (0.025 M) solution followed by crosslinking the solution into a gel by D_2O-based $CaCl_2$ solutions. Four

different calcium concentrations were used including 0.75, 1.1, 1.4 and 2.4 wt. % and 3 batches of different aging periods (5 min, 6 and 48 h) were prepared for all the calcium concentrations (Salomonsen et al., 2009). All samples were freeze dried and rehydrated according to the following procedure: 30 mg of dehydrated alginate powder were rehydrated with 100 µL deuterated water (D_2O). The D_2O (CAS: 7789-20-0, 99.9 atom %) was supplied by Sigma-Aldrich and used as received. All hydrogel samples were freshly prepared and there was no water detected outside the gel (i.e., homogeneous samples with water integrated inside the gel).

All samples were frozen at −80 °C for 6 h and then lyophilized using a bench top freeze dryer (Martin Christ (Osterode am Harz, Germany) Alpha 2–4 LDplus), condenser temperature −80 °C, pressure 100 Pa. The lyophilization time was 48 h for all hydrogels to ensure that not only free water is lyophilized, but also bound water.

2.2. Alginate hydrogels characterization techniques

2.2.1. Cryogenic scanning electron microscopy (Cryo-SEM)

Cryo-scanning electron microscopy was used to visualize the fibrous and porous structure for the alginate gels. Hereto, the field-emission gun scanning electron microscope (JEOL JSM 7100F) equipped with a cryo-transfer system (Quorum PP3000T) operating at an accelerated voltage of 3 keV was used. The cryo- and SEM-stage were conditioned at -140 °C using liquid nitrogen. Prior to sample transfer from the cryo-preparation device to the microscope, the samples were coated with a thin layer of Pt using Argon gas. The samples were mounted on a stub using colloidal graphite/glue 50/50, vitrified in liquid nitrogen and fractured. To reveal the inner microstructure, sublimation at -70 °C for 20 min was applied.

2.2.2. Wide angle X-ray scattering (WAXS) and small angle X-ray scattering (SAXS)

WAXS and SAXS profiles were measured one after another on a Xeuss 3.0 (Xenocs, Grenoble, France) equipped with a Genix 3D Cu-source (λ= 1.54 Å, 50 kV and 0.60 mA) and an Eiger 1M detector (Dectris, Baden, Switzerland). Sample to detector distance was set at 55 and 360 mm respectively. The combined 2θ-range captured varies between 0.01-50 °. The Ca-alginate sample was put in a capillary (WJM glass, Berlin, Germany) after which it was brought in contact with deuterated water to let it hydrate and form the gel. The capillary was sealed with wax and put in a temperature-controlled stage TMHS600 (Linkam, Salfords, United Kingdom) after which it was subjected to a temperature profile (from 20 °C cooled to -85 °C, heated to 40 °C and back cooled to -85 °C, all at 10 °C/min). Acquisition time was set

to 60 s. Furthermore, Na-alginate and the dry Ca-alginate before hydration were measured as reference samples. In this case, acquisition time was set to 600 sec. All profiles were corrected for background intensity, which resulted in an overhead time of about 10% per measurement. Scattering coming from the capillary was subtracted. Graphs were made using Xsact 2.7 (Xenocs, Grenoble, France). Data conversions between q, 2θ and d were made by applying the Bragg's law.

2.2.3. Differential scanning calorimetry (DSC) protocol

All twelve dry alginate powders (5 min, 6 and 48 h aging time with 0.75, 1.1, 1.4 and 2.4 wt. % Ca concentrations) and their hydrogel counterparts were analyzed by DSC. Four samples were weighed from each gel batch with different aging times (i.e., 12 hydrated gel samples in total) and analyzed by DSC. The thermal analysis was performed three times on each individual sample from the 12 total hydrogel samples to ensure reproducibility of the measurements (i.e., 36 total measurements for the 12 hydrogel samples). Thermal analysis was performed using a DSC 25, TA Instruments equipped with a cooling system. 5 mg of each sample were weighed accurately using a micro-balance and the material was then sealed in a Tzero hermetic aluminum pan prior to analysis. Thermogravimetric analysis (TGA) was conducted prior with samples sealed in the hermetic pan to confirm no moisture leakage from the pan. DSC was performed on all samples to investigate the transition temperatures and contents of different water phases (i.e., free, and bound water). The thermal analysis of the dry alginate powders was conducted as a control/reference sample. The samples in the pans were gradually cooled to -85 ^{o}C at 10 ^{o}C.min^{-1} and kept at this temperature for 15 min (i.e., iso-thermal conditions) to ensure all water was frozen. Following that a heating cycle to a final temperature of 40 ^{o}C (using 10 ^{o}C/min ramp) was carried out on the samples followed by a cooling cycle to a final temperature of -85 ^{o}C using the same ramp (i.e., 10 ^{o}C.min^{-1}). 10 cycles from −85 to + 40 °C and back were realized with 10 °C.min^{-1} speed. All the thermograms were normalized (i.e., normalized heat flow). The melting temperatures (T_m) and the corresponding enthalpies ΔH_{endo} (J/g) were determined for each sample as average values over 10 heating cycles.

2.2.4. Fourier transform infrared (FT-IR) spectroscopy

FT-IR was employed in transmittance mode using a Shimadzu IRTracer-100 to ascertain the distinctive functional groups of the dry alginate powders, their hydrogels and pure deuterated water (D_2O). Measurements were conducted within the range of 400 to 4000 cm^{-1}, with 64

scans performed at a resolution of 4 cm^{-1}.

2.2.5. Rheology measurements

The linear viscoelasticity of the alginate-Ca^{2+} hydrogels were determined 5 min, 6 and 48 h after mixing alginate and calcium chloride solutions by small-amplitude oscillatory shear measurements on an Anton Paar MCR302e strain-controlled instrument using a 10 mm diameter cross-hatched stainless-steel plate-plate (PP-10/S), to prevent wall-slip. Stock solutions of alginic acid and $CaCl_2 \cdot 2H_2O$ were injected successively in a 2:1 volume ratio in cylindrical mold (diameter = 10 mm and thickness = 3 mm) to obtain cylindrical hydrogels with flat surfaces with a 3 wt./vol% alginic acid concentration. The hydrogels were then transferred with a spatula on the bottom-plate of the rheometer and squeezed until a gap of 2.8 mm is reached between the top and bottom plates. The exceeding hydrogel parts were carefully cut with a scalpel blade to fit the 10 mm top geometry. All the measurements were performed with a normal force below 0.1 N ensuring full contact between top plate and hydrogel without damaging the hydrogel structure. Strain amplitude measurements from 0.1 to 10 % at a fixed angular frequency of 10 rad/s were first conducted to determine the linear viscoelastic region. Following this step, frequency sweeps were conducted over a range of frequencies from 10 to 0.1 rad/s at fixed strain of 1 %, well within the linear viscoelastic regime. The temperature was controlled via a Peltier cell connected to a recirculating bath and fixed to 20 °C for all the measurements.

3. Results and Discussion

Prior to the characterization and the detection of water phases in the alginate hydrogels, the alginate monomeric fractions and the weight-average molecular weight for the starting material alginic acid was determined using variable temperature Proton NMR spectroscopy and size exclusion chromatography in our previous work (El Hariri El Nokab et al., 2022). The results have shown the following fractions determined to be $F_G = 0.50$, $F_M = 0.50$, $F_{GG} = 0.35$, $F_{GM}=F_{MG} = 0.16$ and $F_{MM} = 0.34$, with an estimated error of ±5%. The weight-average molecular weight ($M_n = 118000$ g/mol, $M_w = 430700$ g/mol) and polydispersity index (PDI) of 3.65 for the alginate. The diverse water pools within the gels were investigated using an array of characterization techniques, including WAXS and SAXS, DSC, FT-IR, rheology,

and Cryo-SEM. The obtained results were subsequently compared to data previously acquired through ssNMR spectroscopy (El Hariri El Nokab et al., 2022).

The prepared hydrogels underwent Cryo-SEM analysis both before and after the sublimation of water droplets, following the method outlined by Aston et al. (Aston et al., 2016). Prior to water sublimation, SEM images depicted in the supplementary material section (**Fig. S1**) for all measured hydrogels reveal a glassy water phase covering the entire surface, seemingly confined within the structure with no droplets adsorbed onto the surface. After water sublimation, the SEM images in **Fig. 1a** illustrate the interconnected fibrous structure of the alginate cryogel, along with the distribution of pores interspersed within the fibrous network.

Following aging, as depicted in **Fig. 1b, d**, the morphological structure undergoes a smoothing effect, with the fibrous wall exhibiting a significant increase in thickness compared to the non-aged samples in **Fig. 1a**. The latter showcases a rough surface and a thinner fibrous wall, approximately 200 nm in thickness, as indicated in the insert. These observed effects are likely attributed to Ostwald's ripening phenomenon, a well-known occurrence in colloid chemistry and material science. In this phenomenon, smaller particles dissolve in the solution upon aging and subsequently re-precipitate onto larger particles, specifically onto the inner walls of the fibrous structure, aiming to attain a stable thermodynamic state.

Conversely, when the calcium concentration is increased to 2.4 wt. %, as shown in **Fig. 1c**, the morphological surface appears rougher, and the interconnected fibrous structure becomes less distinct. These morphological alterations diminish with aging, as illustrated in **Fig. 1d**, where the fibrous structure re-emerges clearly, accompanied by an increase in the degree of crosslinking. The alginate cross linked particles appear in the inserts of **Fig. 1d** where the particle size distribution is uniform and size ranging from 60 to 80 nm, perfectly matching with our previously published data obtained using dynamic light scattering (El Hariri El Nokab et al., 2022; Smaniotto et al., 2020).

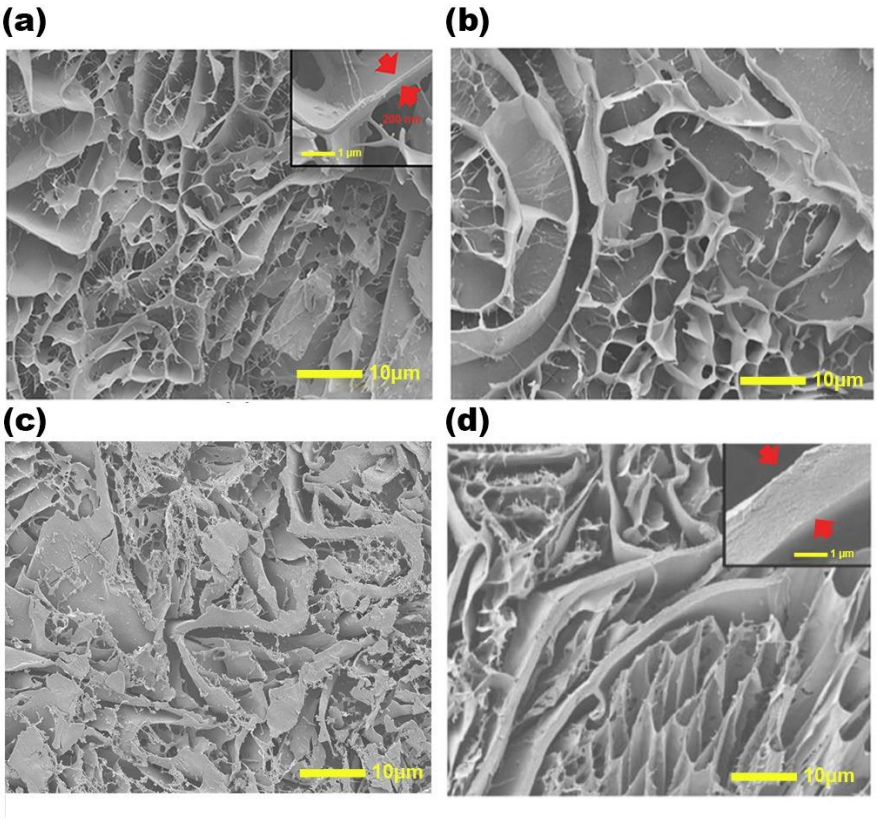

Fig. 1. (a) Cryo-SEM images of (a) 0.75 wt. % Ca alginate hydrogel aged for 5 min, insert for the pore wall thickness. (b) 0.75 wt. % Ca concentration and 48 h aging, (c) 2.4 wt. % Ca concentration and 5 min aging, and (d) 2.4 wt. % Ca concentration and 48 h aging. Insert for the pore wall thickness and the particle size distribution.

Fig. 2a illustrates the behaviour of the hydrated Ca-crosslinked alginate 0.75 wt. % with 6 h aging upon cooling to -85 °C, subsequent heating to 40 °C and once more cooling to -85 °C. The sample with 1.4 wt. % and 48 h aging in **Fig. S2a** was also measured with WAXS, but the profiles encountered where very similar.

At room temperature, the hydrogel was found not to have crystalline material present, as only a liquid-like broad feature was present, situated around 27.5°. The profile change upon hydration of the gel is comparable to the low and high water content gels (Naohara et al., 2017). Already at the third profile, when reaching -3.7 °C, crystalline peaks become present at 23.2°, 24.7°, 26.2°, 34.0°, 40.2° and 44.1°. These peaks signify the formation of water crystals during freezing providing evidence of the presence of free water (Esmaeildoost et al., 2022; Malkin et al., 2012). An overview of the peak positions and their spacings is presented in **Table S1**. The peak intensity increases when cooling further to -85 °C and decreases again when heating to 40 °C is started. The crystalline water peaks remained prevalent until 21.8 °C was reached for 0.75 wt. % - 6 h aging and until 9.6 °C for 1.4 wt. % - 48 h aging. During the

second cooling cycle, the first profile containing the crystalline peaks is around -7.4 °C. A similar profile as for the first cooling cycle was found. The temperatures at which the measurements were conducted were not deliberately selected, but are intrinsically associated with a measurement time of 60 seconds and certain additional overhead time during the measurement process.

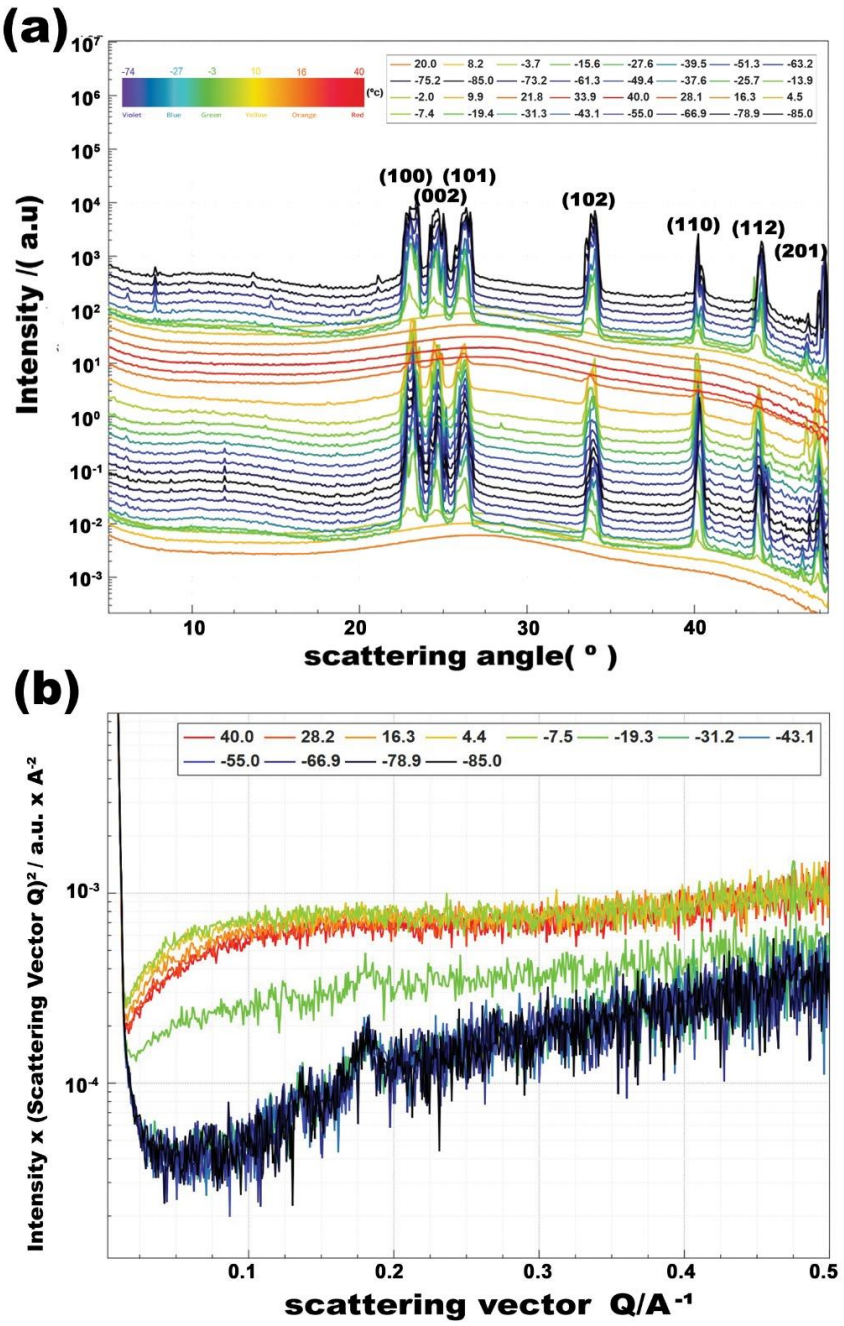

Fig. 2. (a) Variable temperature WAXS experiments with cycle profiles from 20 to -85 °C for the first cycle and then from 40 to -85 °C for the second cycle (b) variable temperature SAXS patterns with same temperature program for 0.75 wt. % Ca alginate 6-h aging hydrogel.

The SAXS analysis of alginate hydrogels presented in **Fig. 2b** and **Fig. S2b** only present the data of the second cooling cycle, i.e. from 40 °C to -85 °C. At 40 °C, for both samples, a clear structure caused by the association of the alginate chains was detected. Upon cooling and crystallization of the water present, the structure disappeared. Nonetheless, in the case of 0.75 wt. % - 6 h aging the peak was identified at approximately 0.10 $Å^{-1}$, while for 1.4 wt. % - 48 h aging the maximum was shifted towards a lower q value of 0.04 $Å^{-1}$. According to the analysis made by (Hermansson et al., 2016), this indicated that the gel with higher Ca^{2+} concentration and longer aging time has a denser structure. It was indeed shown by (Stokke et al., 2000) that the SAXS profiles can change based on the Ca^{2+} concentration.

When freezing the water present in 0.75 wt. % - 6 h aging, two small peaks around q = 0.138 $Å^{-1}$ and 0.183 $Å^{-1}$, consistent with spacings of d = 45.5 Å and 34.3 Å were identified. Although it is unclear where these spacings can be related to, it has been reported before for peaks in the region between 0.1 and 0.2 for alginate gels (Reig-Vano et al., 2023). The formation of the gel and the subsequent freezing of the water was reversible for both samples.

Fig. S2c,d show the WAXS and SAXS data obtained for Na-alginate and the dehydrated Ca-alginate gels 0.75 wt. % with 6 h aging and 1.4 wt. % with 48 h aging. It is clear that the SAXS profiles showed no characteristic features in all cases. On the other hand in WAXS, it can be seen that the Na-alginate profile consists of two broad amorphous-like features, situated around 13.5° and 21.5°. These features were also encountered for samples with low water content (Naohara et al., 2017). Furthermore, no crystalline peaks could be detected. Conversely, WAXS measurements for the dehydrated gels revealed a crystalline peak situated at 32.2° and superimposed upon broad amorphous-like features, indicating the dual nature of the dehydrated Ca-alginate gels.

Polymers, whether natural or synthetic, featuring hydrophilic groups like hydroxyl, carboxyl, and carbonyl groups, as in the case of alginates, exhibit distinct interactions with water, ranging from strong to weak (Guan et al., 2011; Hatakeyama and Hatakeyama, 1998; Hatakeyama et al., 1985; Ostrowska-Czubenko and Gierszewska-Drużyńska, 2009). This interaction significantly impacts the thermal properties of both polymers and water. The characterization of water states within a polymer provides valuable insights into the absorption, diffusion, and permeation properties of hydrophilic materials. The mechanical and physical attributes of hydrophilic materials can undergo significant alterations upon water absorption, attributed to the modification of the polymer chain structure. Differential scanning

calorimetry is a commonly used technique for characterizing such transitions.

Due to phase transition behaviour and molecular mobility (Hatakeyama et al., 1985; Yoshida et al., 1990) during the interaction between water and polymer molecules, three forms of water are classified: (i) *non-freezing bound water*, (ii) *freezing bound water* and (iii) *bulk/free water*. Observing the first-order phase transition of water fractions (i.e., non-freezing bound water) closely associated with the polymer matrix is typically challenging and does not show a phase transition by calorimetric analysis (Yoshida et al., 1993, 1990). Water fractions less closely associated with the polymer matrix demonstrate melting/crystallization, exhibiting considerable supercooling and significantly lower enthalpy compared to bulk/free water. These water fractions are denoted as freezing bound water. The water fractions described as freezing bound water collectively constitute the bound water content when combined with non-freezing water fractions (i.e., total bound water = freezing bound water + non-freezing bound water) (Yoshida et al., 1993, 1992, 1990). Water exhibiting melting/crystallization characteristics like normal (bulk/free) water is termed freezing water. In water-insoluble hydrophilic polymers like alginates, bound water disrupts hydrogen bonding among the hydroxyl groups of the polymer (Hatakeyama and Hatakeyama, 1998). The content of bound water is contingent upon the chemical composition and high-order structure of each polymer and cannot be generalized for all polymers.

Fig. 3a displays the DSC heating thermograms and **Fig. S3** displays both the heating and cooling thermograms, with the melting temperatures and corresponding enthalpies indicated for each melting peak. It is noteworthy to mention that the aqueous solution, whether in bulk or confined within each hydrogel, contains salts essential for the synthesis of the hydrogels. Upon increasing the aging time, the water in the alginate hydrogel sample melts close to the melting temperature of D_2O. This can be seen from the shift in the melting temperature (T_m) upon increasing the aging time of the hydrogel. The freezing bound water's melting temperature (T_m) typically exhibits a lower value than that of bulk/free water, primarily influenced by hydrogen bonding (Guan et al., 2011; Hatakeyama and Hatakeyama, 1998; Ostrowska-Czubenko and Gierszewska-Drużyńska, 2009). However, this T_m may undergo slight changes or remain constant across various polymer/water mixtures (Guan et al., 2011).

More noticeable and important, the melting enthalpies of the three alginate hydrogels (184.6, 196.5 and 208.5 J/g) are lower than the melting enthalpy of pure D2O (340 J/g). This might be attributed to the fact that extending the aging duration of the Ca^{2+} cross-linked alginate from 5 min to 6 h induces the generation of more pores in the alginate microstructure. This alteration prompts a shift in the water pools, causing them to exhibit behaviours more closely

resembling free water, including crystallization, and melting characteristics akin to bulk deuterated water (D_2O). The anticipated consequence of this aging effect is a diminished interaction between water molecules and the walls of interconnected alginate fibers. This process is thought to reach a steady state slightly after 6 h as the ratios of bound to free water do not significantly change between 6 and 48 h of aging. All results including enthalpies, T_m values, and ratios of free/bound water, are summarized in **Table S2**.

Observing the separation of free water and freezable bound water in the cooling cycle poses challenges due to their continuous crystallization process (Buchtová et al., 2018; Guan et al., 2011; Hatakeyama and Hatakeyama, 1998; Hatakeyama et al., 1985; Ostrowska-Czubenko and Gierszewska-Drużyńska, 2009; Yoshida et al., 1993, 1992, 1990). Consequently, heating traces, specifically endothermic peaks, are selected for a quantitative analysis of water content (Buchtová et al., 2018). The results reveal that approximately 54 wt. % of waters within the 5 min aged hydrogel, 58 wt. % within the 6 h aged hydrogel, and 61 wt. % confined in the 48 h aged hydrogel undergo solid-to-liquid phase transition in the explored temperature range (- 85 °C to 40 °C). The remaining water, approximately 46 wt. %, 42 wt. % and 39 wt. % respectively, remains unchanged until at least -85 °C. Overall, DSC analysis indicates that alginate-based hydrogels house confined water exhibiting two distinct physical behaviours, with varying amounts depending on aging time. Generally, confined water undergoing a phase transition near bulk water temperatures is labelled free or bulk-like water (Buchtová et al., 2018). Conversely, water undergoing phase change at different temperatures is categorized as interfacial, "*bound*," or hydration water (Jhon and Andrade, 1973; Li et al., 2008; Qu et al., 2000; Sekine and Ikeda-Fukazawa, 2009).

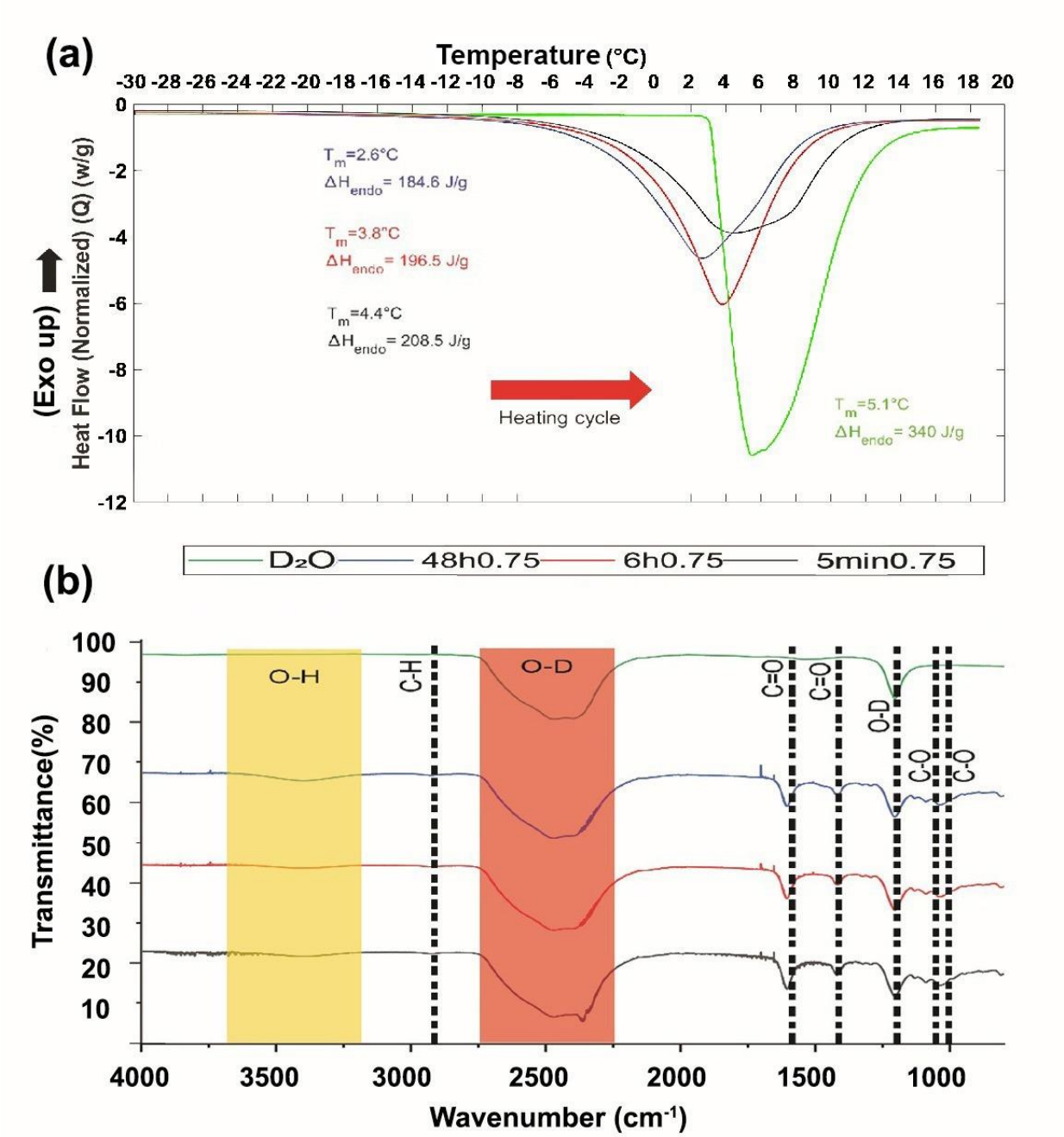

Fig. 3. (a) DSC thermograms of the heating/melting cycle of 1.4 wt. % Ca cross-linked alginate hydrogels at different aging times (5 min, 6 and 48 h). (b) FT-IR data for 0.75 wt. % Ca cross-linked alginate hydrogels at different aging times (5 min, 6 and 48 h). Deuterated water (D2O) was used as a reference sample in both techniques.

In conclusion, the water confined in 6 h aged hydrogel is composed of approx. 58 wt. % of bulk-like water and 42 wt. % of *bound* hydration water. The latter is presumably situated at the interfaces with the hydrophilic hydrogel matrix where it may interact via hydrogen bonding with the alginate polymer chains. Consequently, the behaviour of bound water is modified as referred to the bulk/free-like water. The bound water forms a physical transition

layer between the pore wall of the hydrogel matrix and the bulk-like water which is located far from the interfaces. The amounts of bound water present in alginate-based hydrogels are like the results already reported, like for example in chitosan-based hydrogels (Qu et al., 2000).

FT-IR spectroscopy was performed on alginate hydrogels with different aging times in **Fig. 3b** and various calcium concentrations in **Fig. S4a, b**, then compared to the alginate in powder form in **Fig. S4c, d** and to pure D_2O reference sample in **Fig. 3b**. The alginate shift assignment summarized in **Table S3** includes the O-H stretching appearing as a small peak in the hydrogel at 3400 cm^{-1}, while appearing significantly as a broad peak in the powder samples extended between 3000-3600 cm^{-1} (Daemi and Barikani, 2012). The C-H stretching appears at 2850-2920 cm^{-1}, following that the two peaks at 1650 and 1460 cm^{-1} correspond to the C=O asymmetric and symmetric stretching, respectively (Daemi and Barikani, 2012). The C-O stretching within the pyranose region and the outside appear at 1110 and 1010 cm^{-1}, respectively (Daemi and Barikani, 2012). The O-D stretching and bending peaks (Kim et al., 2002) appear significantly in the alginate hydrogel samples and the pure D_2O reference sample, between 2250-2750 cm^{-1} and 1200 cm^{-1}, respectively (Kim et al., 2002). The O-D stretching could be deconvoluted into overlapped three peaks at 2395, 2479 and 2587 cm^{-1} (Perakis et al., 2016). Upon increasing the aging time negligible difference was detected between the hydrogels, meanwhile upon increasing the calcium concentration the intensity increased for the C-O stretching vibration between 1100-700 cm^{-1} and this could be related to the deformation in the C-C-H and C-O-H stretching mode in the pyranose region of the polymannuronate part of the alginate which could be partially cross-linked with the calcium ions (Daemi and Barikani, 2012).

The formation of alginate hydrogels by mixing alginic acid and $CaCl_2.2H_2O$ was also followed by linear rheology (**Fig. 4**) (Kuo and Ma, 2008). Several ratios between Ca^{2+} and alginic acid were investigated, namely 0.75, 1.1, 1.4 and 2.4 wt. %, and the linear viscoelastic properties of the final hydrogels were measured 5 min, 6 h and 48 h after preparation. First, we can observe that 5 min after mixing alginic acid and Ca^{2+} all the samples already behave rheologically speaking as a hydrogel with a storage modulus (G') overpassing the loss modulus (G'') on the whole range of frequencies investigated (**Fig. 4a**). This indicates the strong and long-lived interactions between Ca^{2+} and G-units that form the "egg-box" structure commonly reported in the literature (Atkins et al., 1973; Grant et al., 1973) In parallel, upon increasing the Ca^{2+} to alginic acid weight ratio from 0.75 to 2.4 wt. %, the stiffness of the

hydrogels increased with plateau moduli values of ≈ 0.6 kPa and ≈ 10 kPa, respectively. This drastic increase reflects the higher density of ionic associations upon increasing the Ca^{2+} content of the hydrogel. Second, after 6 h of aging time, all the prepared hydrogels showed an increase of the stiffness (**Fig. 4b**). While for the hydrogels prepared with 0.75, 1.1 or 1.4 wt. % Ca^{2+} this increase of plateau modulus appears to roughly double (≈ 0.6 kPa to ≈ 1 kPa, ≈ 2.5 kPa to ≈ 5 kPa, ≈ 7 kPa to ≈ 10 kPa, respectively), meanwhile the modulus of the hydrogel prepared with 2.4 wt % Ca^{2+} shows almost a 9-fold increase (from ≈ 10 kPa to ≈ 90 kPa). By further increasing the aging time to 48 h (**Fig. 4c**), no significant change in the linear viscoelastic response was observed for any of the Alg-Ca^{2+} hydrogels, indicating that the maximum crosslinking degree was obtained within the first 6 h after mixing. This aging process is probably due to the limited diffusion speed of the free Ca^{2+} ions within the Alg-Ca^{2+} crosslinked matrix explaining why this process is more prominent at higher Ca^{2+} to alginic acid ratios (Holte et al., 2006; Pasut et al., 2008). The increase in the mechanical properties of the alginate hydrogels upon increasing the Ca^{2+} concentration or the aging time supports Ostward's ripening mechanism (increase in the wall thickness of the interconnecting fibers) which happens during aging periods of several materials in food industry (Khazzar et al., 2023; Nájera et al., 2021).

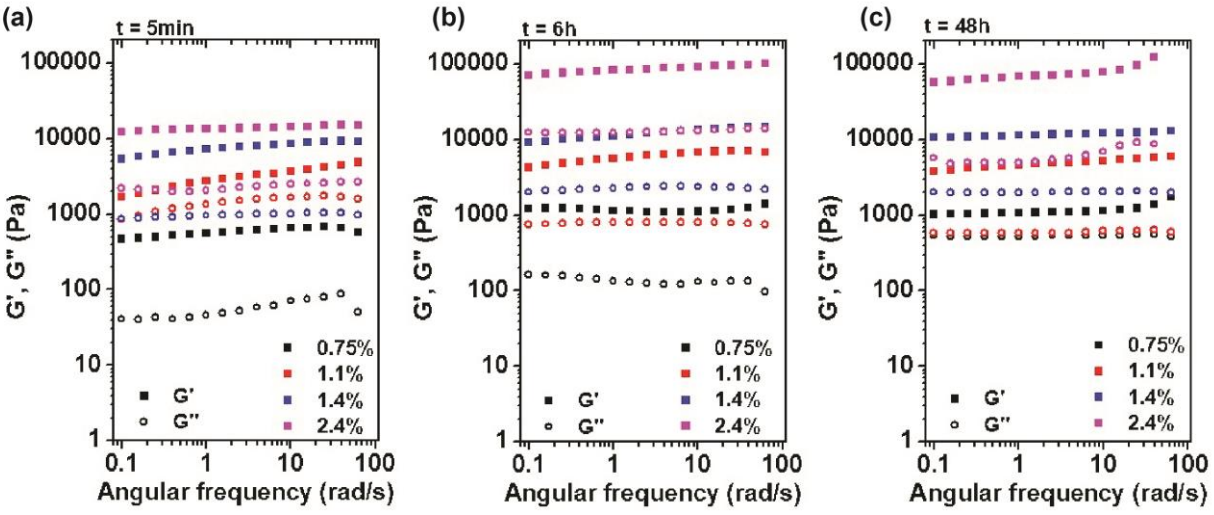

Fig. 4. Linear rheology measurements performed on alginate hydrogels with Ca^{2+} to alginic acid ratios of 0.75, 1.1, 1.4 and 2.4 wt. % at (a) 5 min, (b) 6 h and (c) 48 h aging time.

Alginate is known to serve as an encapsulating material due to its ability to form hydrogels under mild conditions, protecting small drug molecules such as antioxidants from degradation while facilitating controlled release (Pedrali et al., 2023). This encapsulation process involves

the formation of alginate beads or microspheres, where drug molecules are entrapped within the gel matrix. Alginates perform better when chemically modified or mixed with other carbohydrates and proteins.

Modifying alginate can have a significant impact on the behavior of drug molecules encapsulated within it. By altering the chemical composition (e.g., graft modification of alginate) or physical properties of alginate (interactions with other carbohydrates and proteins), the structure can be tuned to enhance the drug release kinetics, gel stability, and release selectivity (Zheng et al., 2007). Chemical modifications like grafting functional groups onto alginate chains can impart specific properties such as photo and pH responsiveness, which can be advantageous for targeted drug delivery to specific sites within the body. Additionally, physical modification such as blending alginate with other carbohydrates or protein polymers e.g., soy protein or whey protein can further tailor the gels properties, thus leading to improved drug loading capacity and enhanced biocompatibility (Pedrali et al., 2023; Zheng et al., 2007).

In the current work we have alternated the crosslinking ion concentration and the aging period (in two different batches) and investigated their effect on the alginate hydrogels. Increasing calcium concentration leads to rougher morphological surfaces and less distinct interconnected fibrous structures, as shown by Cryo-SEM, while aging smoothens the morphological structure and thickens the fibrous wall. WAXS and SAXS analyses revealed the coexistence of amorphous and crystalline phases in Ca-alginate gels, with Variable-Temperature WAXS identifying the transition temperature for water crystal formation, while SAXS indicated that gels with higher Ca^{2+} concentration and longer aging time exhibited denser structures. DSC shows that confined water exhibits two distinct physical behaviors, influenced by aging time, while in FT-IR analysis, increased calcium concentration correlates with crucial structural changes in the poly-MM part essential for Ca^{2+} crosslinking. Linear rheology further indicates that Ca^{2+} enhances hydrogel mechanical strength, reaching peak crosslinking within the initial 6 h post-mixing. Comparing and coupling different analytical techniques (i.e., qualitative versus quantitative approaches) allows us to understand distinct water phases present in alginate hydrogels.

4. Conclusions

In summary, a comparative study was carried out using an array of advanced analytical techniques to compare their capabilities in detecting and quantifying the two water phases in present alginate hydrogels. Alginate hydrogels composed of only 2 wt. % have shown to possess highly porous morphology with interconnected fibrous structure dominating the polymeric region. DSC has shown several advantages over all other techniques regarding its accessibility, rapid testing, and quantitative results in detecting the two different populations of water inside the hydrogel. Meanwhile, all other analytical techniques could perform qualitatively in detecting the free-like water phase which appears confined in the macroporous structure of the hydrogel, but still possesses high mobility at ambient condition and presents the freezing transitions state at around 4 ºC. Cryo-SEM has brought deep insights into the interconnected fibrous structure of the gel where bound-like water phase exists additionally to the macropores where free-like water dominates and possess high mobility. X-ray scattering techniques with variable temperature control units are promising in detecting the different water phases, since water phases with different interactions with their surroundings possess variable freezing points, thus forming different crystallizing structures and using different mechanisms and pathways to crystallize which can be detected easily using the X-ray scattering techniques. Alginate hydrogels are considered promising sustainable materials for the biomedical industry including tissue engineering, drug delivery and wound healing since they have a high ratio of free-like water with high mobility which is beneficial for the diffusion of active pharmaceutical ingredients, nutrients, and waste products, and insures the survivability, migration, and proliferation of the encapsulated cells.

CRediT authorship contribution statement

Mustapha El Hariri El Nokab: Conceptualization, Investigation, Formal analysis, Visualization, Writing – original draft. **Julien Es Sayed:** Investigation, Formal analysis, Visualization. **Fien De Witte:** Conceptualization, Investigation, Formal analysis, Visualization. **Koen Dewettinck:** Supervision. **Ahmed Elshewy:** Conceptualization, Investigation. **Zhenlei Zhang:** Formal analysis. **Paul H. M. Van Steenberge:** Conceptualization. **Tuo Wang:** Writing – review & editing. **Khaled O. Sebakhy:** Conceptualization, Investigation, Formal analysis, Visualization, Supervision, Writing – original draft and Project administration.

Declaration of competing interest

The authors declare that they have no known competing financial interests or personal relationships that could have appeared to influence the work reported in this paper.

Acknowledgements

We would like to thank the Hercules foundation for its financial support in the acquisition of the scanning electron microscope JEOL JSM-7100F equipped with the cryo-transfer system Quorum PP3010T (grant no. AUGE-09-029) used in this research. The Hercules foundation is recognized for funding the Xenocs Xeuss 3.0 X-ray Scattering (XRS) equipment (FWO Hercules Grant AUGE/17/29). Sincere appreciation to the Food Structure & Function Research Group, Ghent University for providing access to SAXS and WAXS. T.W. thanks the support from National Science Foundation (NSF) under the grant number of MCB-2308660. The authors thank Engineer Mohamed Saeed Elgamasy for the artwork provided.

Appendix A. Supplementary data

The following is the Supplementary data to this article: **Fig. S1**. Cryo-SEM images before D_2O sublimation for alginate hydrogels with different Ca concentration and aging time, (a) 0.75 wt. % Ca concentration and 5 min aging, and (b) 2.4 wt. % Ca concentration and 48 h aging. **Fig. S2**. (a) WAXS and (b) SAXS patterns for alginate hydrogel with 1.4 wt. % Ca concentration and 48 h aging time. (c) WAXS and (d) SAXS patterns for sodium alginate powder (alginic acid starting material) and calcium alginate (dehydrated alginate hydrogel). **Table S1**. Wide-angle X-ray scattering peaks assessed for frozen water in Ca-alginate hydrogels. Peaks were assessed based on 0.75 wt. % - 6 h aging gel at -85 °C. **Figure S3**. DSC thermograms of the cooling cycle (upper part: blue arrow) and the heating cycle (lower part: red arrow) of 0.75 wt. % Ca^{2+} cross-linked alginate hydrogels at different aging times (5 min, 6 and 48 h) and the deuterated water (D_2O) as a reference sample for comparison. **Table S2**. Summary of DSC results of different alginate hydrogels. **Fig. S4**. FT-IR sack plots for alginate hydrogels with different Ca concentrations and aging time. (a) 0.75 wt. % Ca concentration hydrogels with different aging time, (b) 2.4 wt. % Ca concentration hydrogels with different aging time (c) 0.75 wt. % Ca concentration powders with different aging time, (b) 2.4 wt. % Ca concentration powders with different aging time. **Table S3**. Peak positions and assignments for FT-IR spectra of alginate hydrogels.

References

Abka-khajouei, R., Tounsi, L., Shahabi, N., Patel, A.K., Abdelkafi, S., Michaud, P., 2022. Structures, Properties and Applications of Alginates. Marine Drugs 20, 364. https://doi.org/10.3390/md20060364.

Agulhon, P., Robitzer, M., David, L., Quignard, F., 2012. Structural Regime Identification in Ionotropic Alginate Gels: Influence of the Cation Nature and Alginate Structure. Biomacromolecules 13, 215–220. https://doi.org/10.1021/bm201477g.

Akamatsu, K., Maruyama, K., Chen, W., Nakao, A., Nakao, S., 2011. Drastic difference in porous structure of calcium alginate microspheres prepared with fresh or hydrolyzed sodium alginate. Journal of Colloid and Interface Science 363, 707–710. https://doi.org/10.1016/j.jcis.2011.08.014.

Amsden, B., 1998. Solute Diffusion within Hydrogels. Mechanisms and Models. Macromolecules 31, 8382–8395. https://doi.org/10.1021/ma980765f.

Andersen, T., Auk-Emblem, P., Dornish, M., 2015. 3D Cell Culture in Alginate Hydrogels. Microarrays 4, 133–161. https://doi.org/10.3390/microarrays4020133.

Aston, R., Sewell, K., Klein, T., Lawrie, G., Grøndahl, L., 2016. Evaluation of the impact of freezing preparation techniques on the characterisation of alginate hydrogels by cryo-SEM. European Polymer Journal 82, 1–15. https://doi.org/10.1016/j.eurpolymj.2016.06.025.

Atkins, E.D.T., Nieduszynski, I.A., Mackie, W., Parker, K.D., Smolko, E.E., 1973. Structural components of alginic acid. II. The crystalline structure of poly-α-L-guluronic acid. Results of X-ray diffraction and polarized infrared studies. Biopolymers 12, 1879–1887. https://doi.org/10.1002/bip.1973.360120814.

Bhujbal, S.V., Paredes-Juarez, G.A., Niclou, S.P., de Vos, P., 2014. Factors influencing the mechanical stability of alginate beads applicable for immunoisolation of mammalian cells. Journal of the Mechanical Behavior of Biomedical Materials 37, 196–208. https://doi.org/10.1016/j.jmbbm.2014.05.020.

Böckmann, A., Gardiennet, C., Verel, R., Hunkeler, A., Loquet, A., Pintacuda, G., Emsley, L., Meier, B.H., Lesage, A., 2009. Characterization of different water pools in solid-state NMR protein samples. J Biomol NMR 45, 319–327. https://doi.org/10.1007/s10858-009-9374-3.

Brus, J., Urbanova, M., Czernek, J., Pavelkova, M., Kubova, K., Vyslouzil, J., Abbrent, S., Konefal, R., Horský, J., Vetchy, D., Vysloužil, J., Kulich, P., 2017. Structure and Dynamics of Alginate Gels Cross-Linked by Polyvalent Ions Probed via Solid State NMR Spectroscopy. Biomacromolecules 18, 2478–2488. https://doi.org/10.1021/acs.biomac.7b00627.

Buchtová, N., D'Orlando, A., Judeinstein, P., Chauvet, O., Weiss, P., Le Bideau, J., 2018. Water dynamics in silanized hydroxypropyl methylcellulose based hydrogels designed for tissue engineering. Carbohydrate Polymers 202, 404–408. https://doi.org/10.1016/j.carbpol.2018.08.143.

Capitani, D., Crescenzi, V., A. A. De Angelis, and, Segre, A.L., 2001. Water in Hydrogels. An NMR Study of Water/Polymer Interactions in Weakly Cross-Linked Chitosan Networks. Macromolecules 34, 4136–4144. https://doi.org/10.1021/ma002109x.

Cavalieri, F., Chiessi, E., Finelli, I., Natali, F., Paradossi, G., Telling, M.F., 2006. Water, Solute, and Segmental Dynamics in Polysaccharide Hydrogels. Macromol. Biosci. 6, 579–589. https://doi.org/10.1002/mabi.200600077.

Daemi, H., Barikani, M., 2012. Synthesis and characterization of calcium alginate nanoparticles, sodium homopolymannuronate salt and its calcium nanoparticles. Scientia Iranica 19, 2023–2028. https://doi.org/10.1016/j.scient.2012.10.005.

Demurtas, D., Guichard, P., Martiel, I., Mezzenga, R., Hébert, C., Sagalowicz, L., 2015. Direct visualization of dispersed lipid bicontinuous cubic phases by cryo-electron tomography. Nat Commun 6, 8915. https://doi.org/10.1038/ncomms9915.

El Hariri El Nokab, M., 2023. Alginate a valuable blend from nature investigated using solid state NMR spectroscopy (PhD thesis). University of Groningen, Groningen. https://doi.org/10.33612/diss.639196779.

El Hariri El Nokab, M., Lasorsa, A., Sebakhy, K.O., Picchioni, F., van der Wel, P.C.A., 2022. Solid-state NMR spectroscopy insights for resolving different water pools in alginate hydrogels. Food Hydrocolloids 127, 107500. https://doi.org/10.1016/j.foodhyd.2022.107500.

El Hariri El Nokab, M., van der Wel, P.C.A., 2020. Use of solid-state NMR spectroscopy for investigating polysaccharide-based hydrogels: A review. Carbohydrate Polymers 240, 116276. https://doi.org/10.1016/j.carbpol.2020.116276.

Esmaeildoost, N., Jönsson, O., McQueen, T.A., Ladd-Parada, M., Laksmono, H., Loh, N.-T.D., Sellberg, J.A., 2022. Heterogeneous Ice Growth in Micron-Sized Water Droplets Due to Spontaneous Freezing. Crystals 12, 65. https://doi.org/10.3390/cryst12010065.

Forgács, A., Papp, V., Paul, G., Marchese, L., Len, A., Dudás, Z., Fábián, I., Gurikov, P., Kalmár, J., 2021. Mechanism of Hydration and Hydration Induced Structural Changes of Calcium Alginate Aerogel. ACS Appl. Mater. Interfaces 13, 2997–3010. https://doi.org/10.1021/acsami.0c17012.

Garcia, H., Barros, A.S., Gonçalves, C., Gama, F.M., Gil, A.M., 2008. Characterization of dextrin hydrogels by FTIR spectroscopy and solid state NMR spectroscopy. European Polymer Journal 44, 2318–2329. https://doi.org/10.1016/j.eurpolymj.2008.05.013.

Gheorghita Puscaselu, R., Lobiuc, A., Dimian, M., Covasa, M., 2020. Alginate: From Food Industry to Biomedical Applications and Management of Metabolic Disorders. Polymers 12. https://doi.org/10.3390/polym12102417.

Grant, G.T., Mon, E.R., Rees, S.D.A., 1973. Biological interactions between polysaccharides and divalent cations: The egg-box model. FEBS LETTERS 32, 195–198. https://doi.org/10.1016/0014-5793(73)80770-7.

Guan, L., Xu, H., Huang, D., 2011. The investigation on states of water in different hydrophilic polymers by DSC and FTIR. Journal of Polymer Research 18, 681–689. https://doi.org/10.1007/s10965-010-9464-7.

Gun'ko, V., Savina, I., Mikhalovsky, S., 2017. Properties of Water Bound in Hydrogels. Gels 3, 37. https://doi.org/10.3390/gels3040037.

Hatakeyama, H., Hatakeyama, T., 1998. Interaction between water and hydrophilic polymers. Thermochimica Acta 308, 3–22. https://doi.org/10.1016/S0040-6031(97)00325-0.

Hatakeyama, T., Nakamura, K., Yoshida, H., Hatakeyama, H., 1985. Phase transition on the water-sodium poly(styrenesulfonate) system. Thermochimica Acta 88, 223–228. https://doi.org/10.1016/0040-6031(85)85433-2.

Hermansson, E., Schuster, E., Lindgren, L., Altskär, A., Ström, A., 2016. Impact of solvent quality on the network strength and structure of alginate gels. Carbohydrate Polymers 144, 289–296. https://doi.org/10.1016/j.carbpol.2016.02.069.

Hoffman, A.S., 2012. Hydrogels for biomedical applications. Advanced Drug Delivery Reviews 64, 18–23. https://doi.org/10.1016/j.addr.2012.09.010.

Holte, O., Tonnesen, H.H., Karlsen, J., 2006. Measurement of diffusion through calcium alginate gel matrices. Pharmazie 61, 30–34.

Jhon, M.S., Andrade, J.D., 1973. Water and hydrogels. Journal of Biomedical Materials Research 7, 509–522. https://doi.org/10.1002/jbm.820070604.

Khazzar, S., Segato, S., Riuzzi, G., Serva, L., Garbin, E., Gerardi, G., Tenti, S., Mirisola, M., Catellani, P., 2023. Influence of Ageing Time and Method on Beef Quality and Safety. Foods 12, 3250. https://doi.org/10.3390/foods12173250.

Kim, J., Schmitt, U.W., Gruetzmacher, J.A., Voth, G.A., Scherer, N.E., 2002. The vibrational spectrum of the hydrated proton: Comparison of experiment, simulation, and normal mode analysis. J. Chem. Phys. 116, 737–746. https://doi.org/10.1063/1.1423327.

Kuo, C.K., Ma, P.X., 2008. Maintaining dimensions and mechanical properties of ionically crosslinked alginate hydrogel scaffolds in vitro. Journal of Biomedical Materials Research Part A 84A, 899–907. https://doi.org/10.1002/jbm.a.31375.

Li, X., Cui, Y., Xiao, J., Liao, L., 2008. Hydrogel–hydrogel composites: The interfacial structure and interaction between water and polymer chains. Journal of Applied Polymer Science 108, 3713–3719. https://doi.org/10.1002/app.27854.

Liparoti, S., Speranza, V., Marra, F., 2021. Alginate hydrogel: The influence of the hardening on the rheological behaviour. Journal of the Mechanical Behavior of Biomedical Materials 116, 104341. https://doi.org/10.1016/j.jmbbm.2021.104341.

Malkin, T.L., Murray, B.J., Brukhno, A.V., Anwar, J., Salzmann, C.G., 2012. Structure of ice crystallized from supercooled water. PNAS 109, 1041–1045. https://doi.org/10.1073/pnas.1113059109.

Meo, C.D., Coviello, T., Matricardi, P., Lamanna, R., 2021. Anomalous enhanced water diffusion in polysaccharide interpenetrating hydrogels. Colloids and Surfaces A: Physicochemical and Engineering Aspects 613, 125892. https://doi.org/10.1016/j.colsurfa.2020.125892.

Miyazaki, T., Kaneko, T., Gong, J.P., Osada, Y., Demura, M., Suzuki, M., 2002. Water-Induced Crystallization of Hydrogels. Langmuir 18, 965–967. https://doi.org/10.1021/la010922v.

Nagaraja, K., Rao, K.M., Rao, K.S.V.K., 2021. Chapter 11 - Alginate-based hydrogels, in: Giri, T.K., Ghosh, B. (Eds.), Plant and Algal Hydrogels for Drug Delivery and Regenerative Medicine. Woodhead Publishing, pp. 357–393. https://doi.org/10.1016/B978-0-12-821649-1.00010-6.

Nájera, A.I., Nieto, S., Barron, L.J.R., Albisu, M., 2021. A Review of the Preservation of Hard and Semi-Hard Cheeses: Quality and Safety. ijerph 18, 9789. https://doi.org/10.3390/ijerph18189789.

Naohara, R., Narita, K., Ikeda-Fukazawa, T., 2017. Change in hydrogen bonding structures of a hydrogel with dehydration. Chemical Physics Letters 670, 84–88. https://doi.org/10.1016/j.cplett.2017.01.006.

Neves, M.I., Moroni, L., Barrias, C.C., 2020. Modulating Alginate Hydrogels for Improved Biological Performance as Cellular 3D Microenvironments. Frontiers in Bioengineering and Biotechnology 8. https://doi.org/10.3389/fbioe.2020.00665.

Noferini, D., Faraone, A., Rossi, M., Mamontov, E., Fratini, E., Baglioni, P., 2019. Disentangling Polymer Network and Hydration Water Dynamics in Polyhydroxyethyl Methacrylate Physical and Chemical Hydrogels. J. Phys. Chem. C 123, 19183–19194. https://doi.org/10.1021/acs.jpcc.9b04212.

Ostrowska-Czubenko, J., Gierszewska-Drużyńska, M., 2009. Effect of ionic crosslinking on the water state in hydrogel chitosan membranes. Carbohydrate Polymers 77, 590–598. https://doi.org/10.1016/j.carbpol.2009.01.036.

Panagopoulou, A., Molina, J.V., Kyritsis, A., Pradas, M.M., Lluch, A.V., Ferrer, G.G., Pissis, P., 2013. Glass Transition and Water Dynamics in Hyaluronic Acid Hydrogels. Food Biophysics 8, 192–202. https://doi.org/10.1007/s11483-013-9295-2.

Pasqui, D., De Cagna, M., Barbucci, R., 2012. Polysaccharide-Based Hydrogels: The Key Role of Water in Affecting Mechanical Properties. Polymers 4, 1517–1534. https://doi.org/10.3390/polym4031517.

Pasut, E., Toffanin, R., Voinovich, D., Pedersini, C., Murano, E., Grassi, M., 2008. Mechanical and diffusive properties of homogeneous alginate gels in form of particles and cylinders. Journal of Biomedical Materials Research Part A 87A, 808–818. https://doi.org/10.1002/jbm.a.31680.

Pedrali, D., Scarafoni, A., Giorgi, A., Lavelli, V., 2023. Binary Alginate-Whey Protein Hydrogels for Antioxidant Encapsulation. Antioxidants 12, 1192. https://doi.org/10.3390/antiox12061192.

Perakis, F., Marco, L.D., Shalit, A., Tang, F., Kann, Z.R., Ku, T.D., Torre, R., Bonn, M., Nagata, Y., 2016. Vibrational Spectroscopy and Dynamics of Water. Chem. Rev. 116, 7590–7607. https://doi.org/10.1021/acs.chemrev.5b00640.

Qu, X., Wirsén, A., Albertsson, A.-C., 2000. Novel pH-sensitive chitosan hydrogels: swelling behavior and states of water. Polymer 41, 4589–4598. https://doi.org/10.1016/S0032-3861(99)00685-0.

Reig-Vano, B., Huck-Iriart, C., de la Flor, S., Trojanowska, A., Tylkowski, B., Giamberini, M., 2023. Structural and mechanical analysis on mannuronate-rich alginate gels and xerogels beads based on Calcium, Copper and Zinc as crosslinkers. International Journal of Biological Macromolecules 246, 125659. https://doi.org/10.1016/j.ijbiomac.2023.125659.

Rodríguez-Suárez, J.M., Butler, C.S., Gershenson, A., Lau, B.L.T., 2020. Heterogeneous Diffusion of Polystyrene Nanoparticles through an Alginate Matrix: The Role of Cross-linking and Particle Size. Environ. Sci. Technol. 54, 5159–5166. https://doi.org/10.1021/acs.est.9b06113.

Roget, S.A., Piskulich, Z.A., Thompson, W.H., Fayer, M.D., 2021. Identical Water Dynamics in Acrylamide Hydrogels, Polymers, and Monomers in Solution: Ultrafast IR Spectroscopy and Molecular Dynamics Simulations. J. Am. Chem. Soc. 143, 14855–14868. https://doi.org/10.1021/jacs.1c07151.

Rossi, B., Venuti, V., D'Amico, F., Gessini, A., Castiglione, F., Mele, A., Punta, C., Melone, L., Crupi, V., Majolino, D., Trotta, F., Masciovecchio, C., 2015. Water and polymer dynamics in a model polysaccharide hydrogel: the role of hydrophobic/hydrophilic balance. Phys. Chem. Chem. Phys. 17, 963–971. https://doi.org/10.1039/C4CP04045G.

Saji, S., Hebden, A., Goswami, P., Du, C., 2022. A Brief Review on the Development of Alginate Extraction Process and Its Sustainability. Sustainability 14, 5181. https://doi.org/10.3390/su14095181.

Salomonsen, T., Jensen, H.M., Larsen, F.H., Steuernagel, S., Engelsen, S.B., 2009. Alginate monomer composition studied by solution- and solid-state NMR – A comparative chemometric study. Food Hydrocolloids 23, 1579–1586. https://doi.org/10.1016/j.foodhyd.2008.11.009.

Sekine, Y., Ikeda-Fukazawa, T., 2009. Structural changes of water in a hydrogel during dehydration. The Journal of Chemical Physics 130, 034501. https://doi.org/10.1063/1.3058616.

Sharma, R., Malviya, R., Singh, S., Prajapati, B., 2023. A Critical Review on Classified Excipient Sodium-Alginate-Based Hydrogels: Modification, Characterization, and Application in Soft Tissue Engineering. Gels 9, 430. https://doi.org/10.3390/gels9050430.

Smaniotto, F., Prosapio, V., Zafeiri, I., Spyropoulos, F., 2020. Freeze drying and rehydration of alginate fluid gels. Food Hydrocolloids 99, 105352. https://doi.org/10.1016/j.foodhyd.2019.105352.

Stokke, B.T., Draget, K.I., Smidsrød, O., Yuguchi, Y., Urakawa, H., Kajiwara, K., 2000. Small-Angle X-ray Scattering and Rheological Characterization of Alginate Gels. 1. Ca−Alginate Gels. Macromolecules 33, 1853–1863. https://doi.org/10.1021/ma991559q.

Tønnesen, H.H., Karlsen, J., 2002. Alginate in Drug Delivery Systems. Drug Development and Industrial Pharmacy 28, 621–630. https://doi.org/10.1081/DDC-120003853.

Urbanova, M., Pavelkova, M., Czernek, J., Kubova, K., Vyslouzil, Jakub, Pechova, A., Molinkova, D., Vyslouzil, Jan, Vetchy, D., Brus, J., 2019. Interaction Pathways and Structure–Chemical Transformations of Alginate Gels in Physiological Environments. Biomacromolecules 20, 4158–4170. https://doi.org/10.1021/acs.biomac.9b01052.

Wang, T., Jo, H., DeGrado, W.F., Hong, M., 2017. Water Distribution, Dynamics, and Interactions with Alzheimer's β-Amyloid Fibrils Investigated by Solid-State NMR. J. Am. Chem. Soc. 139, 6242–6252. https://doi.org/10.1021/jacs.7b02089.

Yoshida, H., Hatakeyama, T., Hatakeyama, H., 1993. Characterization of water in polysaccharide hydrogels by DSC. Journal of Thermal Analysis 40, 483–489. https://doi.org/10.1007/BF02546617.

Yoshida, H., Hatakeyama, T., Hatakeyama, H., 1992. Effect of Water on the Main Chain Motion of Polysaccharide Hydrogels, in: Viscoelasticity of Biomaterials, ACS Symposium Series. American Chemical Society, pp. 217–230. https://doi.org/10.1021/bk-1992-0489.ch014.

Yoshida, H., Hatakeyama, T., Hatakeyama, H., 1990. Phase transitions of the water-xanthan system. Polymer 31, 693–698. https://doi.org/10.1016/0032-3861(90)90291-6.

Zheng, H., Zhou, Z., Chen, Y., Huang, J., Xiong, F., 2007. pH-sensitive alginate/soy protein microspheres as drug transporter. Journal of Applied Polymer Science 106, 1034–1041. https://doi.org/10.1002/app.26725.

Zhou, J., Lin, S., Zeng, H., Liu, J., Li, B., Xu, Y., Zhao, X., Chen, G., 2020. Dynamic intermolecular interactions through hydrogen bonding of water promote heat conduction in hydrogels. Mater. Horiz. 7, 2936–2943. https://doi.org/10.1039/D0MH00735H.